coatings

MDPI

Article

Effect of Mg Addition on Microstructure and Sacrificial Anode Protection Performance of Hot Dip Al-5Zn-4Si-xMg Coating

Zhaobin Liu [1], Jiaxin Li [1,2], Haoping Peng [1,2], Aijun Xie [3] and Zhiwei Li [1,2,3,*]

[1] School of Materials Science and Engineering, Changzhou University, Changzhou 213000, China
[2] School of Petroleum and Natural Gas Engineering, Changzhou University, Changzhou 213000, China
[3] Chemical and Biomolecular Engineering, National University of Singapore, Singapore 119077, Singapore
* Correspondence: lzw@cczu.edu.cn

Abstract: The effect of Mg addition on the microstructure and sacrificial anode protection performance of a hot-dip Al-5Zn-4Si-xMg coating was studied by scanning electron microscopy (SEM-EDS), an X-ray diffractometer, and an electrochemical workstation. The results showed that Al-Zn-Si alloy was composed of an Al-rich phase and a Zn-rich phase. The $MgZn_2$ phase appears after Mg addition. When the addition of Mg increased to 0.15 wt.%, the Mg_2Si phase began to appear in the alloy. The hot-dip Al-5Zn-4Si-xMg coating consisted of Si particles, an Al-rich phase and a Zn-rich phase. When the Mg content increased to 0.15 wt.%, the Mg_2Si phase and Al + Zn + $MgZn_2$ eutectoid phase began to appear in the coating. In the full immersion corrosion test of the hot-dip Al-5Zn-4Si-xMg coating, the order of corrosion resistance was 0.15% Mg coating > 0.2% Mg coating > 0.05% Mg coating > 0 Mg coating. In the corrosion process of the hot-dip Al-5Zn-4Si-0.15Mg coating, with the increase in immersion, the self-corrosion current of the coating decreased, and the sacrificial protection performance was the best.

Keywords: hot-dip aluminizing; sacrificial anode; corrosion resistance

check for updates

Citation: Liu, Z.; Li, J.; Peng, H.; Xie, A.; Li, Z. Effect of Mg Addition on Microstructure and Sacrificial Anode Protection Performance of Hot Dip Al-5Zn-4Si-xMg Coating. *Coatings* **2023**, *13*, 1087. https://doi.org/10.3390/coatings13061087

Academic Editor: Alexander Modestov

Received: 20 March 2023
Revised: 13 April 2023
Accepted: 31 May 2023
Published: 12 June 2023

Copyright: © 2023 by the authors. Licensee MDPI, Basel, Switzerland. This article is an open access article distributed under the terms and conditions of the Creative Commons Attribution (CC BY) license (https://creativecommons.org/licenses/by/4.0/).

1. Introduction

Hot-dip aluminizing and its alloy coating is an effective method of steel corrosion protection [1] that is widely used in home appliances, rail transits, and construction fields [2,3]. At present, Al-Si (Al-10Si), Al-Mg-Si, and Al-Zn-Si (Galvalume, 55Al-43.4Zn-1.6Si) are relatively mature aluminum-rich coatings. In order to increase the fluidity, Si is generally added to the molten pool. The Al-Si alloy coating is composed of an aluminum-rich phase and a silicon-rich phase [4]. The Mg element can be introduced into the Al-Mg-Si alloy to form an Al-Mg_2Si quasi-eutectic structure, Al, Fe-Al master alloy, and Mg_2Si ternary eutectic structure [5]. The Al-Zn-Si alloy coating is mainly composed of an aluminum-rich phase and a zinc-rich phase. During the condensation process, the aluminum-rich phase with a large amount of Zn was dissolved preferentially. With the decrease in the temperature, the Al-rich phase was continuously precipitated in the Zn-rich phase. Therefore, there were Al-rich particles in the Zn-rich phase [6] and spangles between the Zn-rich dendrites [7].

The ideal alloy coating should have a sacrificial protection performance, reasonable speed corrosion, and the ability to form corrosion products with protective properties [8,9]. In the natural environment, the aluminum coating is passivated by forming a dense and partially hydrated oxide layer to provide good barrier protection for the coating. However, passivation also leads to the loss of sacrificial protection performance [10,11]. In a low chloride environment, the spontaneous passivation of Al reduces the efficiency of the aluminum coating to protect the steel [12,13]. In the high chloride environment, aluminum is subjected to localized corrosion [14], reducing the coating efficiency. Therefore, it is necessary to find a better-quality aluminum coating.

The alloying of the Al coating is an alternative strategy [15,16]. In the Al-based coating, the sacrificial protection can be improved by adding alloying elements to destroy the oxide

film and reduce its corrosion potential. The alloy coating can also form new corrosion products to provide a supplementary self-healing effect [8,9]. Si can effectively reduce the thickness of the Fe-Al alloy layer [17,18]. However, Si particles also precipitate in the coating, which aggravates the corrosion of the coating to some extent [16]. In order to obtain good coating quality, a Si content of 4%–6% is most appropriate. When more than 5% Si is used, the processing performance decreases significantly [19]; therefore, the Si content in this study was selected at 4%. Zn addition can reduce the self-corrosion potential of the Al-rich coating [20]. In the study of Al-Zn-Si coating, A, V, Paramonov [21] believed that 4%–6% of Zn had better corrosion resistance. Therefore, this study selected the Zn content of 5%. Mg was also considered to reduce the corrosion potential of the aluminized layer. According to the research of Gao et al., the addition of Mg to the Al-Zn-Si alloy could make the self-corrosion potential shift positively, increase the corrosion resistance of the alloy coating, and thus improve its corrosion resistance [11]. Cheng et al. [13] believed that when the coating did not contain Mg or the content of Mg was less than 0.1%, ZnO and basic zinc carbonate were produced during the corrosion of the coating, which could not effectively protect the matrix. In order to improve the corrosion resistance, an appropriate amount of Mg needed to be added to inhibit the formation of such products. Magnesium compounds have good corrosion resistance. Adding Mg can also reduce the area of the Zn-rich phase and reduce the effective area of corrosion, thereby improving its corrosion resistance. In view of the effect of Mg on the corrosion of the Al-Zn-Si coating, Liu [16] added 1%–4% Mg to a Galvalume alloy for a detailed study. However, the addition of Mg led to a large amount of the $MgZn_2$ phase being enriched on the surface of the coating, which was not conducive to ensuring the stability of the coating. Therefore, it is meaningful to further reduce the addition of Mg and study the effect of trace Mg addition on the microstructure of the coating. In addition, the mechanism of Mg improving the corrosion resistance of aluminum coating has not been unified. Therefore, it is necessary to study the mechanism of Mg addition to improve the corrosion resistance of the Al coating.

In this study, Al-5Zn-4Si-xMg (x = 0, 0.05, 0.15, and 0.2 wt.%) alloy coatings were designed and prepared. The phase composition and microstructure of the coating were analyzed by X-ray diffraction (XRD) and scanning electron microscope (SEM-EDS). The corrosion resistance was evaluated by a long-term immersion test and electrochemical test in a 3.5 wt.% NaCl solution. This provided a theoretical basis for further understanding the effect of Mg on the corrosion products and corrosion behavior of aluminum-rich coatings. At the same time, it also provided a basis for the development of an aluminum coating with sacrificial anode protection performance.

2. Materials and Methods

2.1. Preparation of Al-5Zn-4Si-xMg Alloy Coating

Q235 steel with a size of 10 mm × 20 mm × 3 mm was used as the substrate. Table 1 lists the chemical composition of Q235 steel. The steel substrate was successively polished, degreased by alkali washing with 80 °C NaOH solution and rusted by pickling with a 10 wt.% HCl solution, and pre-treated by fluxing at 87 °C. The NH_4Cl-$ZnCl_2$-KCl-$SnCl_2$ solution (170 g/L, 230 g/L, 100 g/L, 50 g/L) with a concentration of 200–300 g/L was selected as the flux, and the fluxing time was 5 min. The sample needed to be dried at 100 °C for 10 min to enter the zinc bath. The zinc bath was prepared from 99.9 wt.% industrial pure zinc, 99.99 wt.% pure magnesium particles, Al-24%Si intermediate alloy, and 99.7% industrial pure aluminum. The dipping time was 10, 20, 40, 60, 120 and 180 s, respectively. Slowly the dipped sample was lifted out of the zinc bath and immediately immersed in water to cool it [22,23].To avoid the contingency of the experiment, in the same method, three samples were processed at a time, and each method was repeated three times.

Table 1. Chemical composition of Q235 steel (wt.%).

Chemical Composition	C	Si	Mn	S	P	Fe
Content, wt.%	0.12	0.18	0.5	0.045	0.04	Bal.

For the Al-5Zn-4Si-xMg coating, the addition of the trace of Mg could improve the anode protection performance of the coating. In order to determine the additional amount of Mg, the isothermal section of the Al-Zn-Si-Mg quaternary alloy was calculated by Fact Sage software, as shown in Figure 1. From the high-temperature region to the low-temperature region, there were liquid, liquid + FCC, FCC + Silicon, FCC + Silicon + Mg_2Si, FCC + Silicon + $MgZn_2$, and Silicon + $MgZn_2$ + FCC. During the cooling and solidification process, the Mg_2Si phase was formed by condensation in the alloy liquid. Additionally, the higher the amount of Mg added, the more prone it was to the Mg_2Si phase. Therefore, the addition of Mg was determined to be 0, 0.05%, 0.15%, and 0.2% Mg.

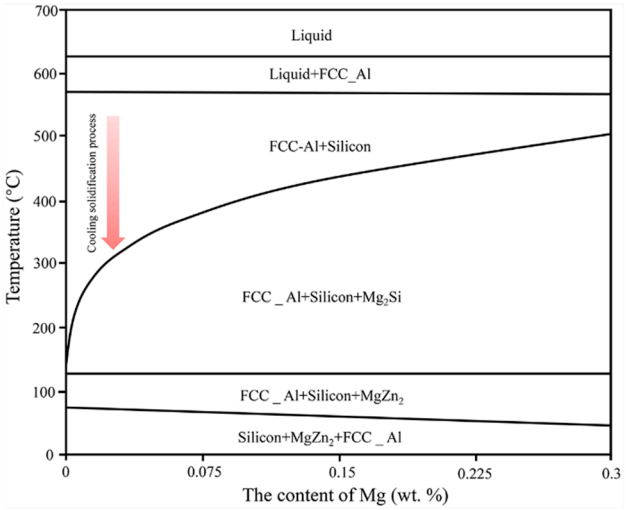


Figure 1. The isothermal section of Al-Zn-Si-Mg quaternary alloy.

2.2. Characterization of Al-5Zn-4Si-xMg Coating

The surface and cross-section of the coating were selected as the observation surface, and the metallographic observation was carried out after epoxy resin cold inlay → rough grinding → fine grinding → diamond polishing paste polishing → 4% nitric acid alcohol solution corrosion → anhydrous ethanol cleaning → blow drying.

The microstructure of the coating surface and cross-section was observed by a JEOL-6510 scanning electron microscope (SEM). The composition of the coating was analyzed by an energy dispersive spectrometer (EDS). The phase was identified by X-ray diffraction (XRD). The tube current was 30 mA, and the working voltage was 45 kV. The single-color Cu radiation method was used = 1.5406 Å, and the penetration depth was ~5 μm.

2.3. Full Immersion Corrosion of Al-5Zn-4Si-xMg Coating

The cold-set samples were immersed in a 3.5 wt.% NaCl solution prepared by deionized water and a full immersion corrosion test was performed to evaluate the corrosion rate of the coating. They were weighed with an electronic balance before immersion. A total of 480 h of immersion corrosion was carried out every 120 h during this period before the samples were wiped with alcohol and dried and then weighed on an electronic balance. The corrosion rate was calculated by the difference between the weight before and after.

2.4. Electrochemical Corrosion of Al-5Zn-4Si-xMg Coating

The electrochemical corrosion behavior of the alloy coating was studied by an electrochemical workstation (CHI660). Corrview software (CView 3.10) was used to fit the data,

and the error was within 5%. Potentiodynamic polarization analysis was performed for a three-electrode system. The auxiliary electrode was a platinum sheet, and the reference electrode was a saturated calomel electrode (SCE). According to the experimental needs, the area of the working electrode was designed to be 1 cm^2. All samples were measured in a naturally aerated 3.5 wt.% NaCl solution without stirring. At room temperature, all electrochemical tests were performed at 30 min after the open circuit potential (OCP) was stabilized. Potentiodynamic polarization curves were measured at a scan rate of 1 mV/s from −0.5 V to +0.5 V vs. OCP. To ensure accuracy, each experiment was performed with five identical samples.

3. Results and Discussion

3.1. Effect of Mg Content on Molten Bath of Al-5Zn-4Si-xMg Alloy

Figure 2 shows the microstructure of the Al-5Zn-4Si-xMg alloy. Table 2 lists the EDS analysis results of phase composition in the alloy. It could be seen from the quaternary phase diagram in Figure 1 that Mg_2Si and $MgZn_2$ phases could appear in the Al-5Zn-4Si-xMg alloy. The phase composition of the quaternary alloy could be determined by the difference in the microstructure and EDS analysis results. The Al-5Zn-4Si mainly contained a gray massive Al-rich phase and white dendritic Zn-rich phase. After the addition of Mg, the number of white dendritic Zn-rich phases in the molten bath increased sharply, and the $MgZn_2$ phase appeared. This was because $MgZn_2$ had a high nucleation rate in the liquid phase. When Mg was introduced into the molten pool, Mg preferentially bonded with Zn. When the Mg content was low, a white bright Zn-rich phase was formed. When the Mg content increased to 0.15 wt.%, the black dotted Mg_2Si phase began to appear in the molten bath. This was because the nucleation rate of the Mg_2Si phase was second only to the $MgZn_2$ phase [15]. At this time, in addition to bonding with Zn to form the $MgZn_2$ phase, rich Mg also bonded with Si to form the Mg_2Si phase. When the Mg content increased to 0.20 wt.%, the number of the Mg_2Si phase in the molten bath decreased, and the network $MgZn_2$ phase appeared. This was because, with the increase in the Mg content, the sufficient supply of Mg in the molten bath made the $MgZn_2$ phase continue generating, which resulted in the formation of a lamellar $MgZn_2$ phase. The consumption of Mg also reduced the number of Mg_2Si phases.

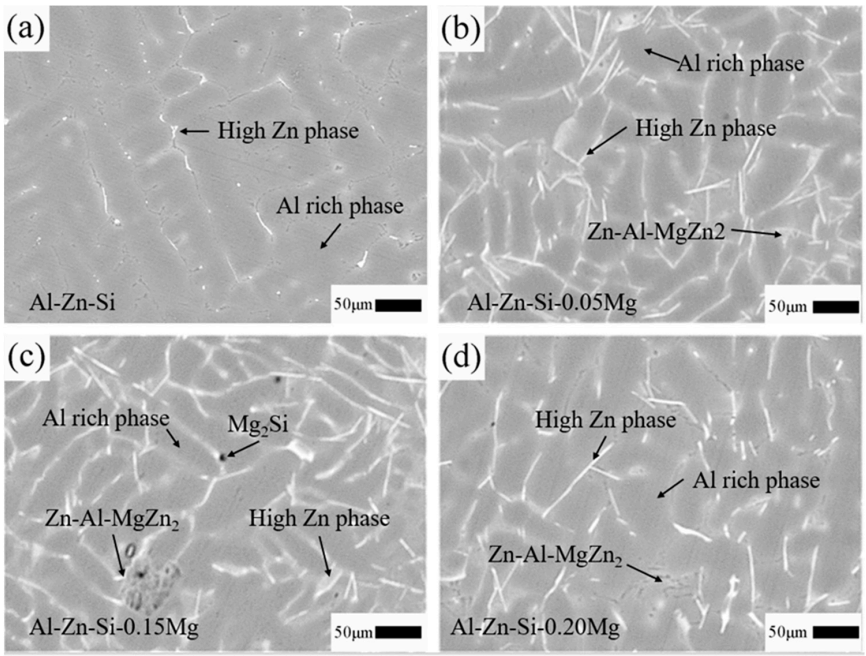


Figure 2. Secondary electron diagram of the microstructure of the Al-5Zn-4Si-xMg alloy after condensation: (**a**) 0.00 wt.% Mg; (**b**) 0.05 wt.% Mg; (**c**) 0.15 wt.% Mg; (**d**) 0.2 wt.% Mg.

Table 2. EDS analysis results of each alloy phase composition in the molten bath, wt.%.

Zinc Alloy Bath	Phase	Composition, wt.%			
		Al	**Zn**	**Si**	**Mg**
Al-Zn-Si	Al rich phase	82.1	10.5	7.4	-
	High Zn phase	4.0	85.3	10.7	-
Al-Zn-Si-0.05Mg	Al rich phase	73.1	20.5	6.4	-
	High Zn phase	5.6	82.6	10.3	1.5
	Zn-Al-$MgZn_2$	5.9	80.4	0.2	14.5
Al-Zn-Si-0.15Mg	Al rich phase	73.6	20.7	5.7	-
	High Zn phase	6.1	82.0	10.4	1.5
	Zn-Al-$MgZn_2$	8.8	94.6	1.2	15.4
	Mg_2Si	3.4	1.0	33.7	61.9
Al-Zn-Si-0.20Mg	Al rich phase	79.3	10.6	10.1	-
	High Zn phase	3.3	84.5	10.1	2.1
	Zn-Al-$MgZn_2$	2.1	79.7	0.1	18.1

3.2. Effect of Mg Content on Microstructure of Hot-Dip Al-5Zn-4Si-xMg Coating

Figure 3 shows the surface morphology of the hot-dip Al-5Zn-4Si-xMg coating. It can be seen from Figure 3a that the surface of the hot-dip Al-Zn-Si coating easily formed on a cracked Al_2O_3 oxide film. The film on the surface of the Al-Zn-Si coating was discontinuous and accompanied by a small number of holes, which were caused by the shrinkage of the surface aluminum liquid during solidification. After adding Mg, the compactness of the coating surface film increased, and the number of holes decreased. With the increase in the Mg content, the crack characteristics of the surface film of the hot-dip Al-5Zn-4Si-xMg coating decreased first and then increased, and the compactness of the film also decreased first and then increased. When the additional amount of Mg was 0.15 wt.%, the compactness of the coating surface was the best.

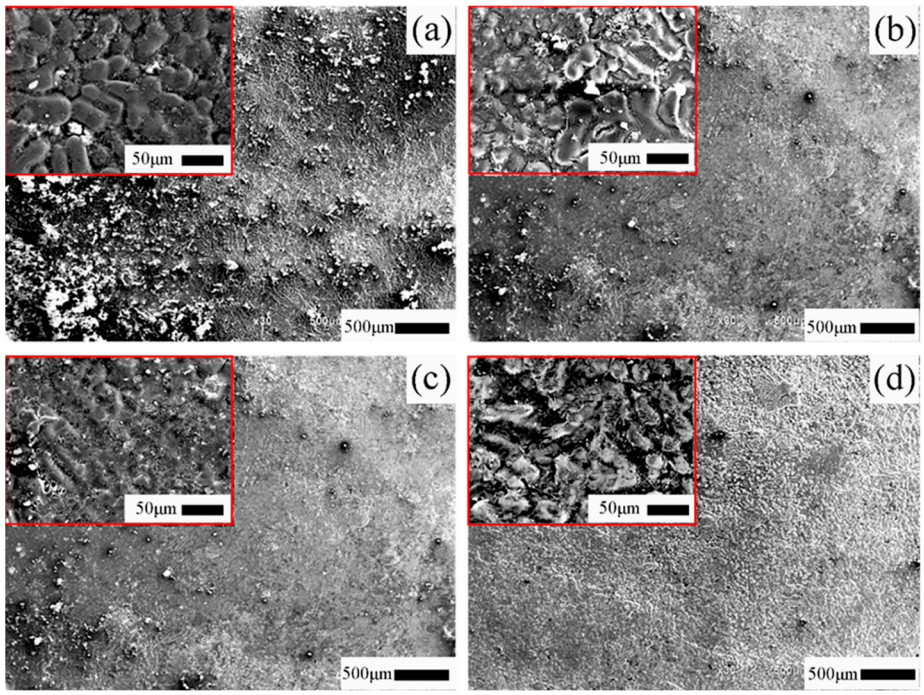


Figure 3. Secondary electron diagram of the surface morphology of the hot-dip Al-5Zn-4Si-xMg coating: (**a**) 0.00 wt.% Mg; (**b**) 0.05 wt.% Mg; (**c**) 0.15 wt.% Mg; (**d**) 0.2 wt.% Mg.

Figure 4 shows the X-ray diffraction pattern of the hot-dip Al-5Zn-4Si-xMg (x = 0, 0.05, 0.15, 0.2) coating surface. For the coatings with a different Mg content, the Al-rich

phase was basically composed of Al (2θ: 28.472, 44.738, 65.133, 78.227), and only a small amount of Al was oxidized to form an Al_2O_3 oxide film (2θ: 17.653). A small amount of Si formed SiO_2 (2θ: 28.438, 79.392). Some Mg combined with Al to form Mg-Al oxides, and the characteristic peaks of Zn, Mg_2Si, and $MgZn_2$ were weak, while some peaks overlapped with other peaks.

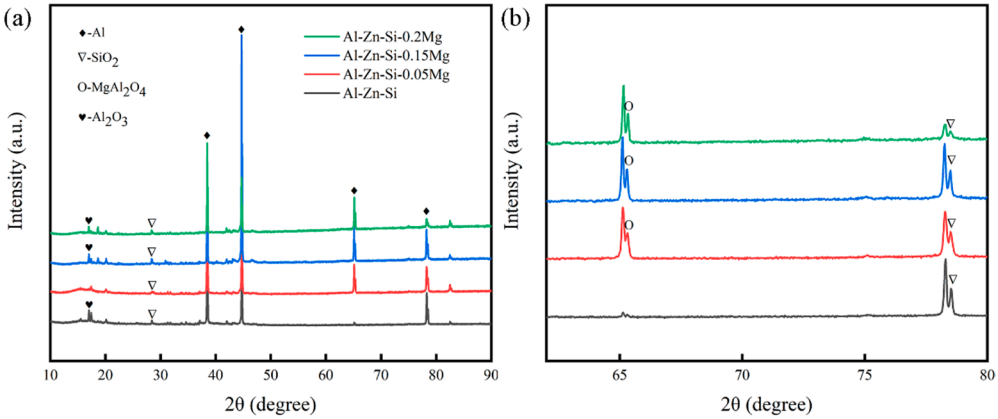


Figure 4. (**a**) X-ray diffraction patterns of hot-dip Al-5Zn-4Si-xMg (x = 0, 0.05, 0.15, 0.2) coatings, (**b**) local magnified graph in (**a**).

Figure 5 shows the cross-section microstructure of the hot-dip Al-5Zn-4Si-xMg coating. There were three parts, including the free layer, the Fe-Al alloy layer, and the Q235 substrate from the surface to the inside of the coating. According to the calculation results of Figure 1, combined with the microstructure and EDS analysis results, the phase composition of the coating could be judged. The intermetallic compounds in the alloy layer of the four coatings were basically the same, all of which were Fe-Al intermetallic compounds. In addition, it can be seen from Figure 5 that the free layer dominated the coating, and the thickness of the Fe-Al alloy layer was very thin. Therefore, this section focuses on the free layer and analyzes the effect of different additions of Mg on the phase composition of the free layer.

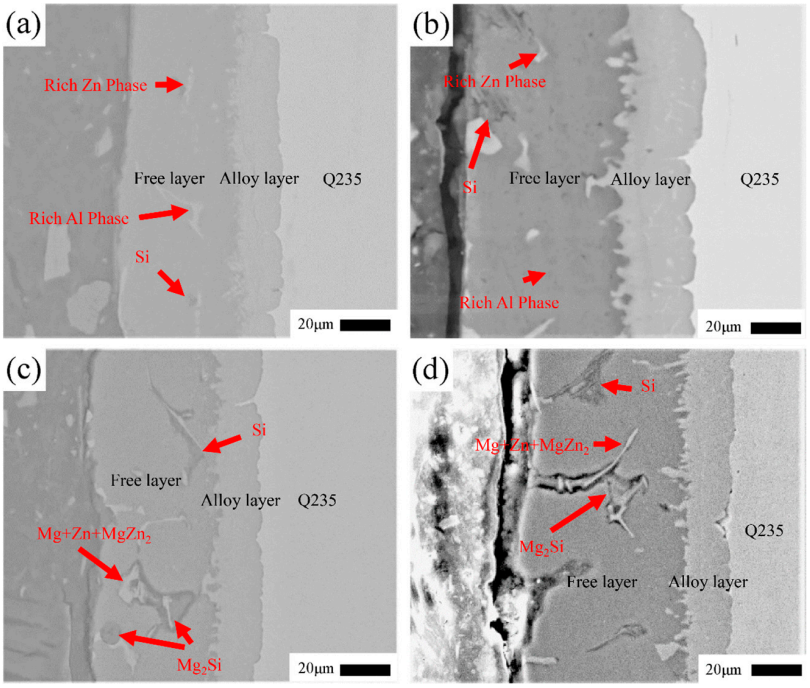


Figure 5. Backscattering diagram of the cross-section microstructure of hot-dip Al-5Zn-4Si-xMg coating: (**a**) 0.00 wt.% Mg; (**b**) 0.05 wt.% Mg (**c**) 0.15 wt.% Mg; (**d**) 0.20 wt.% Mg.

As shown in Figure 5a, there were Si particles, an Al-rich phase, and a Zn-rich phase in the Al-Zn-Si coating. The white stripe was the Zn-rich phase. Si was distributed in the interdendritic region. As shown in Figure 5b, after adding 0.05 wt.% Mg, the alloy layer was still composed of Si particles, an Al-rich phase, and a Zn-rich phase. However, compared with Al-Zn-Si, the number of white Zn-rich phases in the Al-Zn-Si-0.05Mg coating increased, which was caused due to the adsorption of Zn by Mg. As shown in Figure 5c, an obvious Mg_2Si phase and Al + Zn + $MgZn_2$ eutectoid structure appeared in the alloy layer when the Mg content increased to 0.15 wt.%. The Al-Zn eutectic structure was transformed into an Al-Zn-$MgZn_2$ eutectoid structure. As shown in Figure 5d, when the Mg content increased to 0.20 wt.%, the Mg_2Si phase and Al + Zn + $MgZn_2$ eutectoid structure also appeared in the alloy layer. However, compared with Al-Zn-Si-0.15Mg, the number of the Mg_2Si phase in the Al-Zn-Si-0.2.0Mg coating decreased, which was consistent with the composition of the alloy molten bath.

3.3. Full Immersion Corrosion of Hot-Dip Al-5Zn-4Si-xMg Coating

Table 3 lists the results of the full immersion corrosion of the hot-dip Al-5Zn-4 Si-xMg coating in a 3.5 wt.% NaCl solution for 20 days. After 20 days of the full immersion corrosion experiment, the weight of each group of samples increased by varying degrees. This was because the coating underwent oxygen absorption and hydrogen evolution corrosion during immersion corrosion. Corrosion products covered the surface of the coating, resulting in an increase in the weight of the sample. From the average corrosion rate, with the increase in the Mg content, the corrosion resistance of the coating increased first and then decreased. When the addition of Mg was less than 0.15 wt.%, the corrosion resistance of the coating showed an increasing trend. This was because, with the increase in the Mg addition, the Mg-rich phase compounds in the coating increased, resulting in an increase in the corrosion resistance of the coating. When the addition of Mg was 0.15 wt.%, the corrosion resistance of the coating was the best. This was because there were the Mg-Zn-$MgZn_2$ eutectoid structure and Mg_2Si alloy phase in the coating. The presence of the alloy phase increased the impedance response of the coating, thus showing the best corrosion resistance. When the addition of Mg was higher than 0.15 wt.%, the corrosion resistance of the coating decreased. This could be because when the Mg content was 0.20 wt.%, the number of Mg_2Si alloy phases decreased due to the enrichment of Mg-the Zn-$MgZn_2$ eutectoid structure in the coating, which reduced the diversity of the alloy phases in the coating. This led to a decrease in the corrosion resistance of the coating. From the above analysis, the order of the corrosion resistance of the hot-dip Al-5Zn-4Si-xMg coating was 0.15% Mg coating > 0.2% Mg coating > 0.05% Mg coating > 0 Mg coating.

Table 3. The results of hot-dip Al-5% Zn-4% Si-xMg coating immersed in 3.5% NaCl solution for 20 days.

Test Specimen	Before Corrosion (g)	After Etching (g)	Average Corrosion Rate (g/m^2·h)
Al-Zn-Si	12.6076 ± 0.0005	12.6168 ± 0.0004	0.1917
Al-Zn-Si-0.05Mg	11.1925 ± 0.0002	11.1989 ± 0.0006	0.1306
Al-Zn-Si-0.15Mg	12.6603 ± 0.0003	12.6626 ± 0.0005	0.0479
Al-Zn-Si-0.20Mg	13.3902 ± 0.0003	13.3933 ± 0.0005	0.0645

In order to confirm the above speculation, an X-ray diffractometer was used to analyze the corrosion products of the coating surface after 20 days of corrosion, as shown in Figure 6. Comparing the four groups of the products, it was shown that there were strong peaks at 20°, 38.5°, and 45° in the four groups, corresponding to SiO_2, Al, and $Zn(OH)_2$, respectively. This shows that Si and Zn in the coating were corroded, and Al was partially corroded. In the Al-Zn-Si sample, there was an obvious Al_2O_3 peak, while the Al_2O_3 peak intensity in the other samples was weak. This indicates that, compared with the Al-Zn-Si sample, the corrosion degree of Al in the coating with the Mg addition was lighter. In addition, no

Mg-containing corrosion products were found on the surface of the coating when the Mg content was less than 0.15 wt.%. When the addition of Mg was greater than or equal to 0.15 wt.%, Mg corrosion products such as $Mg(OH)_2$ and $Mg_2Al_4Si_5O_{18}$ were found on the surface of the coating. Moreover, the intensity of the Al_2O_3 characteristic peak decreased with an increase in the Mg content. This indicated that the Mg-rich phase in the coating participated in the corrosion of the coating and played a sacrificial role in protecting the Al coating. When the addition of Mg increased to 0.20 wt.%, the intensity of the $Mg_2Al_4Si_5O_{18}$ characteristic peak on the surface of the coating decreased, indicating that the sacrificial protection of the Mg-rich phase was weakened, which is consistent with the conclusion that the number of the Mg_2Si alloy phase found in the coating to be decreased.

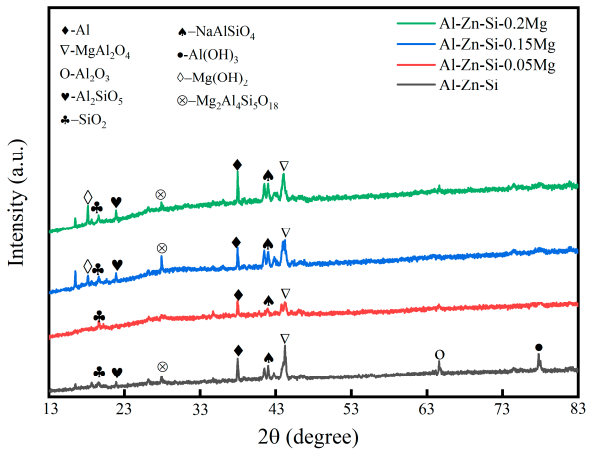


Figure 6. X-ray diffraction pattern of corrosion products on the surface of hot-dip Al-5Zn-4Si-xMg coating after 20 days of corrosion.

The corrosion products were removed by 5% nitric acid alcohol, and the surface morphology of the coating after corrosion was obtained, as shown in Figure 7. As shown in Figure 7a, the coating without Mg showed a crack morphology after corrosion, and there were cracks on the surface of the coating. As shown in Figure 7b, after adding 0.05 wt.% of Mg, the number of cracks on the surface of the corroded coating decreased, and the compactness of the coating increased. As shown in Figure 7c, after adding 0.15 wt.% Mg, no cracks were found on the surface of the corroded coating, and the coating was uniform and complete, showing the best corrosion resistance. As shown in Figure 7d, the coating after corrosion remained intact after adding 0.20 wt.% Mg, but a small number of small cracks could be found on the surface of the coating. It can be seen from the above analysis that after the addition of Mg, the Mg-rich phase in the coating was preferentially corroded, which plays a sacrificial protective role in the coating. When the additional amount of Mg was 0.15 wt.%, the coating exhibited the best corrosion resistance.

3.4. Potentiodynamic Polarization of Hot-Dip Al-5Zn-4Si-xMg Coating in 3.5 wt.% NaCl Solution

From the above analysis, the Al-Zn-Si-0.15Mg alloy coating had the best corrosion resistance. Therefore, Figure 8 shows the potentiodynamic polarization curves of the Al-Zn-Si-0.15Mg coating after immersion corrosion for different time periods. For the Al-5Zn-4Si-0.15Mg coating, the cathode was oxygen absorption corrosion and hydrogen evolution corrosion during immersion corrosion. The anode was the dissolution of magnesium-rich, zinc-rich, and aluminum-rich phases [24]. With the increase in the immersion time, the polarization curve moved to the left as a whole. Table 4 lists the self-corrosion parameters of hot-dip Al-Zn-Si-0.15Mg in different time periods. During the corrosion process of the 0.15Mg coating alloy, its self-corrosion potential moved to a more negative direction with the extension of the immersion time, and the potential remains in the sacrificial anode protection potential range. In the Mg-containing alloy coating, Zn and Mg were alloyed to

form an Mg-Zn-$MgZn_2$ eutectoid structure [25]. Mg and Si formed the more active Mg_2Si phase and reduced the number of silicon inclusions. An excessive Si was still retained in the form of metal inclusions [26]. Mg_2Si and $MgZn_2$ became priority corrosion sites to improve the sacrificial protection performance. Mg^{2+} made it easier to form dense corrosion products on the coating surface. In addition, to the medium containing Cl^-, the solid Mg at the interface promoted the absorption of Cl^-, which could activate the aluminum anode. It could be seen from the above analysis that the Mg-containing alloy coating had the following advantages of improving the corrosion resistance of the coating: (1) the selective dissolution of the Mg-rich phase provided sacrificial protection for the Al side [27]; (2) Mg acted as an electron transfer barrier and played a direct protective role, thus reducing the corrosion rate [28,29]; (3) The surrounding Mg ions inhibited the direct precipitation of Zn corrosion products and increased the compactness of the coating [30–32]. When the additional amount of Mg was 0.15 wt.%, the Mg-rich in the coating was evenly distributed, and the number was large so that the coating exhibited the best corrosion resistance.

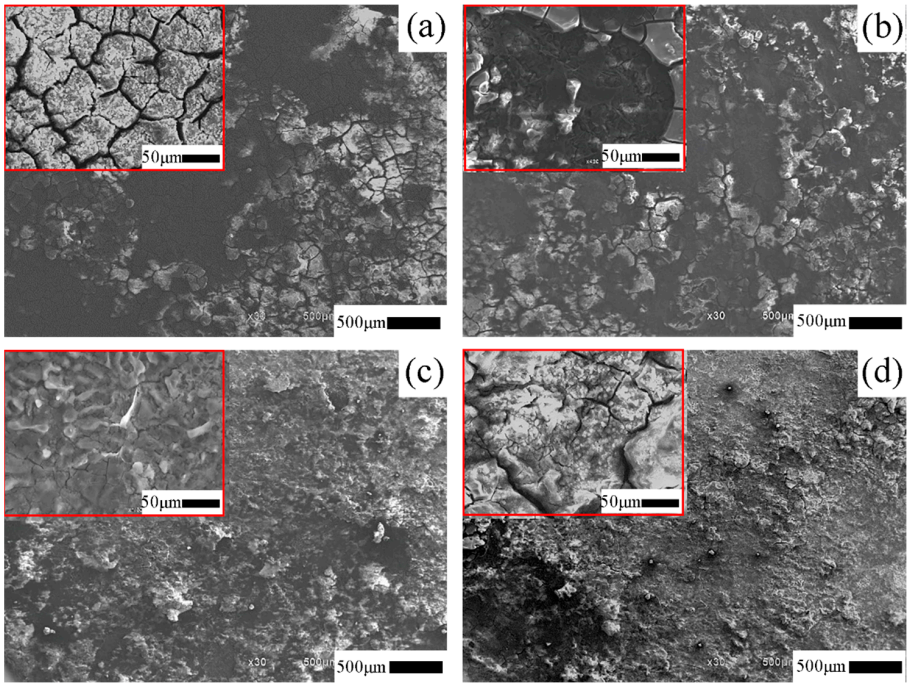


Figure 7. Secondary electron diagram of the surface morphology of the Al-5Zn-4Si-xMg coating after corrosion: (**a**) 0.00 wt.% Mg; (**b**) 0.05 wt.% Mg; (**c**) 0.15 wt.% Mg; (**d**) 0.20 wt.% Mg.

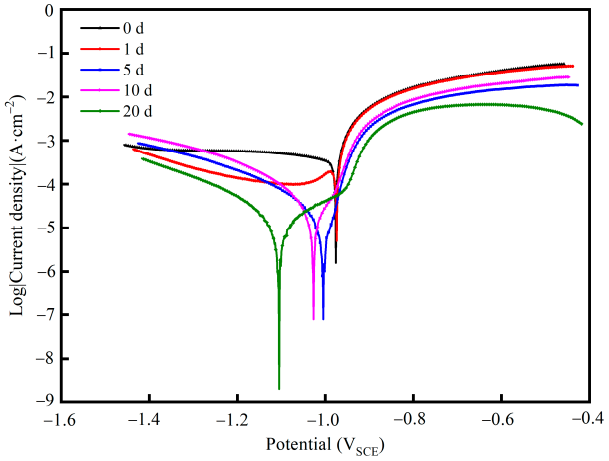


Figure 8. Polarization curves of hot-dipped Al-Zn-Si-0.15Mg at different immersion corrosion times.

Table 4. Self-corrosion parameters of hot-dipped Al-Zn-Si-0.15Mg at different immersion times.

Time (Day)	E_{corr} (V)	I_{corr} (A/cm^2)
0	−0.9756	2.0721×10^{-4}
1	−0.9770	1.3055×10^{-4}
5	−1.0278	1.1769×10^{-5}
10	−1.0036	5.1363×10^{-6}
20	−1.1039	1.1164×10^{-6}

4. Conclusions

(1) The Al-Zn-Si alloy was composed of an Al-rich phase and a Zn-rich phase. The $MgZn_2$ phase appeared after Mg addition. When the addition of Mg increased to 0.15 wt.%, the Mg_2Si phase began to appear in the alloy.

(2) The hot-dip Al-5Zn-4Si-xMg coating was composed of Si particles, an Al-rich phase, and a Zn-rich phase. When the Mg content increased to 0.15 wt.%, Mg_2Si phase and Al + Zn + $MgZn_2$ eutectoid structure appeared in the coating.

(3) The order of corrosion resistance of the hot-dip Al-5Zn-4Si-xMg coating for the full immersion corrosion test was 0.15% Mg coating > 0.2% Mg coating > 0.05% Mg coating > 0 Mg coating. In the corrosion process of hot-dipAl-5Zn-4Si-0.15Mg coating, with the increase in immersion, the self-corrosion current of the coating decreased, and the sacrificial protection performance was the best.

Author Contributions: Conceptualization, Z.L. (Zhiwei Li) and H.P.; methodology, Z.L. (Zhaobin Liu); software, Z.L. (Zhiwei Li); validation, H.P., A.X. and Z.L. (Zhiwei Li); formal analysis, J.L.; investigation, Z.L. (Zhaobin Liu); resources, J.L.; data curation, Z.L. (Zhaobin Liu); writing—original draft preparation, Z.L. (Zhaobin Liu); writing—review and editing, Z.L. (Zhiwei Li); visualization, A.X.; supervision, H.P.; project administration, H.P.; funding acquisition, Z.L. (Zhaobin Liu) and J.L. All authors have read and agreed to the published version of the manuscript.

Funding: Financial support from the Postgraduate Research & Practice Innovation Program of Jiangsu Province (KYCX20-2514 and KYCX23-3142).

Institutional Review Board Statement: Not applicable.

Informed Consent Statement: Not applicable.

Data Availability Statement: Not applicable.

Conflicts of Interest: The authors declare no conflict of interest.

References

1. Tsuru, T. Hot-dipped Al-Mg-Si Coating Steel—Its Structure, Electrochemical and Mechanical Properties. *Corros. Sci. Technol.* **2010**, *9*, 233–238.
2. Huilgol, P.; Rajendra Udupa, K.; Udaya Bhat, K. Formation of microstructural features in hot-dip aluminized AISI 321 stainless steel. *Int. J. Miner. Metall. Mater.* **2018**, *25*, 190–198. [CrossRef]
3. Yuan, X.; Zhang, Q. Microstructure Evolution of Hot-Dip Al-10% Si Coating During the Austenitization of 22MnB5 Hot Stamping Steel. *Acta Metall. Sin.* **2017**, *53*, 1495–1503.
4. Liu, H.-H.; Cheng, W.-J.; Wang, C.-J. The mechanism of oxide whisker growth and hot corrosion of hot-dipped Al–Si coated 430 stainless steels in air–NaCl(g) atmosphere. *Appl. Surf. Sci.* **2011**, *257*, 10645–10652. [CrossRef]
5. Kyo, Y.; Yadav, A.P.; Nishikata, A.; Tsuru, T. Hydrogen entry behaviour of hot-dip Al–Mg–Si coated steel. *Corros. Sci.* **2011**, *53*, 3866–3871. [CrossRef]
6. Moreira, A.R.; Panossian, Z.; Camargo, P.L.; Moreira, M.F.; Da Silva, I.C.; De Carvalho, J.R. Zn/55Al coating microstructure and corrosion mechanism. *Corros. Sci.* **2006**, *48*, 564–576. [CrossRef]
7. Li, Z.; Peng, H.; Liu, Y.; Su, X.; Kawi, S.; Wang, J. Synergy of ball-milling and pre-oxidation on microstructure and corrosion resistance of hot-dip zinc coating of nodular cast iron. *J. Mater. Res. Technol. JmrT* **2022**, *16*, 1402–1412. [CrossRef]
8. Zeng, F.L.; Wei, Z.L.; Li, J.F.; Li, C.X.; Xing, T.A.; Zhang, Z.; Zheng, Z.Q. Corrosion mechanism associated with Mg_2Si and Si particles in Al–Mg–Si alloys. *Trans. Nonferr. Met. Soc. China* **2011**, *21*, 2559–2567. [CrossRef]
9. Thébault, F.; Vuillemin, B.; Oltra, R.; Ogle, K.; Allely, C. Investigation of self-healing mechanism on galvanized steels cut edges by coupling SVET and numerical modeling. *Electrochim. Acta* **2008**, *53*, 5226–5234. [CrossRef]

10. Allely, C.; Dosdat, L.; Clauzeau, O.; Ogle, K.; Volovitch, P. Anticorrosion mechanisms of aluminized steel for hot stamping. *Surf. Coat. Technol.* **2014**, *238*, 188–196. [CrossRef]
11. Gao, J.W.; Wen, J.B.; He, J.G. The Research of Electrochemical Properties of Al-Mg-Sn-Ga-Bi Alloys in Alkaline Electrolyte. *Adv. Mater. Res.* **2013**, *800*, 488–491. [CrossRef]
12. Li, Z.; Peng, H.; Xie, A.; Wu, C.; Kawi, S.; Wang, J. Effect of ball-milling pretreatment on microstructure and corrosion of hot-dip galvanized coating. *Mater. Charact.* **2022**, *192*, 112177. [CrossRef]
13. Cheng, W.-J.; Wang, C.-J. Microstructural evolution of intermetallic layer in hot-dipped aluminide mild steel with silicon addition. *Surf. Coat. Technol.* **2011**, *205*, 4726–4731. [CrossRef]
14. Alvarez-Pampliega, A.; Lamaka, S.V.; Taryba, M.G.; Madani, M.; De Strycker, J.; Tourwé, E.; Ferreira, M.G.; Terryn, H. Cut-edge corrosion study on painted aluminum rich metallic coated steel by scanning vibrating electrode and micro-potentiometric techniques. *Electrochim. Acta* **2012**, *61*, 107–117. [CrossRef]
15. Li, S.; Gao, B.; Tu, G.; Hu, L.; Sun, S.; Zhu, G.; Yin, S. Effects of magnesium on the microstructure and corrosion resistance of Zn–55Al–1.6Si coating. *Constr. Build. Mater.* **2014**, *71*, 124–131. [CrossRef]
16. Liu, W.; Li, M.C.; Luo, Q.; Fan, H.Q.; Zhang, J.Y.; Lu, H.S.; Chou, K.C.; Wang, X.L.; Li, Q. Influence of alloyed magnesium on the microstructure and long-term corrosion behavior of hot-dip Al–Zn–Si coating in NaCl solution. *Corros. Sci.* **2016**, *104*, 217–226. [CrossRef]
17. Li, Z.; Peng, H.; Liu, Y.; Wang, J.; Su, X. Effect of Surface Micromorphology and Roughness of Iron Ingot on Microstructures of Hot-Dip Galvanized Coating. *Trans. Indian Inst. Met.* **2021**, *75*, 397–406. [CrossRef]
18. Li, Z.; Ruan, R.; Xi, S.; Wang, J.; Lei, Y.; Deng, S.; Su, X.; Peng, H. The Influence of Al on the Surface Properties of the Hot-dip Galvanized Melt. *J. Wuhan Univ. Technol. Mater. Sci. Ed.* **2022**, *37*, 117–122. [CrossRef]
19. Gao, C.; Gao, M.; Wang, P. Study on the Inhibitory Effect of Silicon on Steel/Aluminum Rolling Composite Interfacial Compounds. *J. Shenyang Norm. Univ. Nat. Sci. Ed.* **2010**, *28*, 185–188.
20. Breslin, C.B.; Carroll, W.M. The activation of aluminium by activator elements. *Corros. Sci.* **1993**, *35*, 197–203. [CrossRef]
21. Paramonov, A.V.; Adamov, A.S.; Chernetsov, V.Y. Production problems of hot dip galvanized metal structures. *Metallurgist* **2011**, *54*, 793–796. [CrossRef]
22. Khalaj, G.; Khalaj, M.-J. Modeling layer thickness of duplex ceramic (chromium carbonitride) coating on cold work tool steel using fuzzy logic. *J. Intell. Fuzzy Syst.* **2014**, *26*, 2229–2237. [CrossRef]
23. Khalaj, G.; Khalaj, M.-J. Application of ANFIS for modeling of layer thickness of chromium carbonitride coating. *Neural Comput. Appl.* **2014**, *24*, 685–694. [CrossRef]
24. Zhang, G.; Song, R.; Liu, J.; Zhao, S.; Cai, C. Effect of Mg content on structure and corrosion behavior of novel hot-dip Al-Zn-Si-rE-Mg coatings. *Mater. Lett.* **2022**, *328*, 133098. [CrossRef]
25. Takata, N.; Nishimoto, M.; Kobayashi, S.; Takeyama, M. Morphology and formation of Fe–Al intermetallic layers on iron hot-dipped in Al–Mg–Si alloy melt. *Intermetallics* **2014**, *54*, 136–142. [CrossRef]
26. Birbilis, N.; Buchheit, R.G. Electrochemical Characteristics of Intermetallic Phases in Aluminum Alloys. *J. Electrochem. Soc.* **2005**, *152*, B140. [CrossRef]
27. Salgueiro Azevedo, M.; Allély, C.; Ogle, K.; Volovitch, P. Corrosion mechanisms of Zn(Mg,Al) coated steel: The effect of HCO_3^- and NH_4^+ ions on the intrinsic reactivity of the coating. *Electrochim. Acta* **2015**, *153*, 159–169. [CrossRef]
28. Prosek, T.; Nazarov, A.; Bexell, U.; Thierry, D.; Serak, J. Corrosion mechanism of model zinc–magnesium alloys in atmospheric conditions. *Corros. Sci.* **2008**, *50*, 2216–2231. [CrossRef]
29. Diler, E.; Lescop, B.; Rioual, S.; Vien, G.N.; Thierry, D.; Rouvellou, B. Initial formation of corrosion products on pure zinc and $MgZn_2$ examinated by XPS. *Corros. Sci.* **2014**, *79*, 83–88. [CrossRef]
30. Prosek, T.; Persson, D.; Stoulil, J.; Thierry, D. Composition of corrosion products formed on Zn–Mg, Zn–Al and Zn–Al–Mg coatings in model atmospheric conditions. *Corros. Sci.* **2014**, *86*, 231–238. [CrossRef]
31. Salgueiro Azevedo, M.; Allély, C.; Ogle, K.; Volovitch, P. Corrosion mechanisms of Zn(Mg, Al) coated steel in accelerated tests and natural exposure: 1. The role of electrolyte composition in the nature of corrosion products and relative corrosion rate. *Corros. Sci.* **2015**, *90*, 472–481. [CrossRef]
32. Salgueiro Azevedo, M.; Allély, C.; Ogle, K.; Volovitch, P. Corrosion mechanisms of Zn(Mg,Al) coated steel: 2. The effect of Mg and Al alloying on the formation and properties of corrosion products in different electrolytes. *Corros. Sci.* **2015**, *90*, 482–490. [CrossRef]

Disclaimer/Publisher's Note: The statements, opinions and data contained in all publications are solely those of the individual author(s) and contributor(s) and not of MDPI and/or the editor(s). MDPI and/or the editor(s) disclaim responsibility for any injury to people or property resulting from any ideas, methods, instructions or products referred to in the content.